Spin–orbit coupling for tidally evolving super-Earths

A. Rodríguez,[1*] N. Callegari, Jr,[2] T. A. Michtchenko[1] and H. Hussmann[3]

[1]*Insituto de Astronomia, Geofísica e Ciências Atmosféricas, IAG-USP, Rua do Matão 1226, 05508-900 São Paulo, Brazil*
[2]*Instituto de Geociências e Ciências Exatas, Unesp-Univ Estadual Paulista, Av. 24-A, 1515, 13506-900 Rio Claro, SP, Brazil*
[3]*German Aerospace Centre (DLR), Institute of Planetary Research, Rutherfordstr. 2, 12489 Berlin, Germany*

ABSTRACT

We investigate the spin behaviour of close-in rocky planets and the implications for their orbital evolution. Considering that the planet rotation evolves under simultaneous actions of the torque due to the equatorial deformation and the tidal torque, both raised by the central star, we analyse the possibility of temporary captures in spin–orbit resonances.

The results of the numerical simulations of the exact equations of motions indicate that, whenever the planet rotation is trapped in a resonant motion, the orbital decay and the eccentricity damping are faster than the ones in which the rotation follows the so-called pseudo-synchronization. Analytical results obtained through the averaged equations of the spin–orbit problem show a good agreement with the numerical simulations.

We apply the analysis to the cases of the recently discovered hot super-Earths Kepler-10 b, GJ 3634 b and 55 Cnc e. The simulated dynamical history of these systems indicates the possibility of capture in several spin–orbit resonances; particularly, GJ 3634 b and 55 Cnc e can currently evolve under a non-synchronous resonant motion for suitable values of the parameters. Moreover, 55 Cnc e may avoid a chaotic rotation behaviour by evolving towards synchronization through successive temporary resonant trappings.

Key words: celestial mechanics – planets and satellites: general.

1 INTRODUCTION

Tidal theories have gained great attention in the last decade due to the large number of discovered close-in planets which orbit their parent stars with periods of a few days. According to classical theories (e.g. Darwin 1880; Kaula 1964; Mignard 1979), the long-term tidal evolution of these planets results in orbital decay and circularization, on time-scales which depend on the physical properties of the interacting systems (Hut 1981; Dobbs-Dixon, Lin & Mardling 2004; Ferraz-Mello, Rodríguez & Hussmann 2008; Jackson, Barnes & Greenberg 2009; Rodríguez & Ferraz-Mello 2010).

The rotation of short-period planets is also affected by tidal interactions. It is nowadays accepted that the spin rate of planets soon after their formation was much higher than their orbital mean motion (e.g. Agnor, Canup & Levison 1999; Kokubo & Ida 2007). However, the cumulative tidal effects cause the planet to spin down, reaching its stationary value in time-scales much shorter than those needed to circularize the planet orbit. This evolution ultimately results in the synchronous rotation (the spin state in which the orbital and rotation periods coincide), which occurs when the planet orbit is circularized (Hut 1981; Ferraz-Mello et al. 2008). For non-circular

orbits, the synchronous rotation only occurs if an additional torque acts to counteract the tidal torque.

The additional gravitational torque may be generated by planets with a rocky-like composition having a permanent equatorial deformation or frozen-in figure (see Goldreich & Peale 1966; Greenberg & Weidenschilling 1984). These torques, in contrast to the tidal ones, are conservative. In the context of the two-body problem, the gravitational interaction of the star with an asymmetric planet drives the planet rotation into different regimes of motion, including oscillations around exact spin–orbit resonances (SORs; Goldreich & Peale 1966). When dissipative tidal effects are taken into account, the oscillations are damped and the planet rotation is trapped into a resonance. Indeed, the rotational motion of some Solar system bodies can be explained by the combined effects of the tidal and asymmetric torques (Goldreich & Peale 1966; Greenberg & Weidenschilling 1984; Correia & Laskar 2009).

Mercury is an example of a rocky planet with a rotation state currently evolving in the 3/2 SOR (Pettengill & Dyce 1965). Several models of the secular spin evolution of Mercury have been developed, including (i) the chaotic evolution of its orbit (Correia & Laskar 2004), (ii) effects of the core-mantle friction (Correia 2006; Correia & Laskar 2009), (iii) the evolution starting with retrograde and subsequent synchronous motion combined with impact events (Correia & Laskar, 2012; Wieczorek et al. 2012) and (iv) the consideration of non-linear tidal theories (Makarov 2012). However,

despite a lot of previous works, the question that how the current resonant state of Mercury was achieved still remains under discussion.

Concerning the rotation of Earth-like close-in extrasolar planets, a near synchronous motion is usually assumed in view of tidal evolution. However, Correia, Levrard & Laskar (2008) have shown that when an additional torque is considered, the equilibrium rotation of tidally evolved planets can assume rotational states which depart from synchronism. Moreover, as the capture probability in a non-synchronous SOR requires a non-circular orbit (Goldreich & Peale 1966; Celletti & Chierchia 2008), the rotation of several recently discovered super-Earth planets in eccentric orbits can be currently evolving under a resonant motion, provided the planet figure can support a permanent equatorial deformation. As the eccentricity is tidally damped, several resonant trappings would become unstable and the planet rotation ultimately reaches synchronization for almost circular orbits. However, the locking in a non-synchronous resonance with the very short orbital period can protect certain planet longitudes from solar radiation, providing more favourable conditions with respect to habitability as compared to non-resonant rotation (Dobrovolskis 2007). Moreover, Heller, Leconte & Barnes (2011) studied the equilibrium rotation of super-Earths and the implications on their habitability. They found that, under the assumption of an evolution driven by tidal torques, the equilibrium value of the rotation period of GJ 581 d is probably about two times smaller than the orbital period.

In a recent work, Callegari & Rodríguez (2012) have analysed the rotation of extrasolar planets with orbital periods less than 33 d and masses below the mass of Neptune. Depending on one parameter related to the equatorial ellipticity and also on the orbital eccentricity, they identified regions of chaotic rotation in the phase space of some particular planets like 55 Cnc e, GJ 1214 b, Gliese 876 d, among others.

The present investigation aims at two main aspects: (i) how the orbital evolution of the planet, due to tidal interaction with the central star, is altered when the asymmetric torque is considered; and (ii) to analyse the occurrence of captures in spin–orbit resonant motions under combined effects of both torques for the planets Kepler-10 b, 55 Cnc e and GJ 3634 b. These planets are examples of hot super-Earths, which are close-in planets having a few Earth-masses with a rocky composition. We are interested in the past behaviour in the history of the rotation and the subsequent evolution to synchronization. We also discuss the possibility of a current evolution of the rotation of these planets into a super-synchronous resonance state. Moreover, we investigate the implications on the orbital evolution due to such temporary resonant trappings.

Despite the continuously growing number of discovered planets, their rotation state and equilibrium figures remain unknown. In this work, we perform several numerical simulations of the evolution of the systems, assuming several values of unknown parameters, such as equatorial ellipticity and initial rotation. The results allow us to understand the past history of these systems, their current orbital configuration and final rotational states. It should be noted that the majority of previous works concerning spin–orbit interactions with tidal dissipation have been addressed in the context of a fixed Keplerian orbit, with constant values of semi-major axis and eccentricity (e.g. Celletti, Froeschlé & Lega 2007; Celletti & Chierchia 2008). This assumption is adequate for Solar system bodies, where tidal interactions are weak and, consequently, variations of orbital elements are small.

On the other hand, the existence of extrasolar planets with orbital periods of a few days indicates that their current orbital configu-

rations would be the consequence of strong tidal interaction with the host star. In this case, the Keplerian approximation is no longer valid. Thus, we analyse spin–orbit interactions as the orbit evolves due to tidal effects. Solving the exact equations of motion of the problem, we show that the forces arising from the potential of an asymmetric planet also contributes to the orbital variation, accelerating the orbital decay and the eccentricity damping, but only in the cases in which the rotation is locked in resonance.

The spin–orbit problem can also be modelled by the use of averaged equations of motion, where only terms with secular and resonant arguments are retained (e.g. Celletti & Chierchia 2008; Correia & Laskar 2009). Through this model, we compute the averaged variations of semi-major axis and eccentricity due to the combination of asymmetric and tidal forces. We also give an explicit expression for the critical value of the equatorial prolateness, for which a given SOR would become unstable. The study of the particular cases of 2/1, 3/2 and 1/1 SORs indicates a good agreement with the results of the numerical simulations of the exact equations.

This paper is structured as follows. In Section 2, we present the exact equations of motion of the spin–orbit problem. Section 3 shows the results of the numerical simulations, illustrating the evolutions of Kepler-10 b, GJ 3634 b and Cnc 55 e. We show that, assuming a non-zero value of the equatorial ellipticity, different temporary resonant trappings of the rotation can occur, with implications in the orbital decay and circularization. An analytical approach in the context of the averaged equations is shown in Section 4, explaining the results obtained in the numerical simulations. Finally, Section 5 is devoted to discussion and conclusions.

2 THE MODEL

We consider a planet orbiting a central star with a period of a few days. Hereafter, we refer to m and M as the planet and star masses, respectively; R and r as the planet radius and the instantaneous star–planet distance, respectively. The elements a, e and n stand for the semi-major axis, eccentricity and mean motion of the astrocentric orbit of the planet, respectively.

We suppose that the rotating planet body can be approximated by a homogeneous triaxial ellipsoid, with the equatorial axes $\hat{a}$ and $\hat{b}$ and the rotation axis $\hat{c}$. We assume that $\hat{a} > \hat{b} > \hat{c}$ and $\hat{c}$ is normal to the orbital plane (i.e. no obliquity is considered; planar problem). In addition, we assume that the equatorial asymmetry ($\hat{a} \neq \hat{b}$) corresponds to a frozen-in body or permanent deformation of the planet. The assumption above can be supported under consideration of a rocky composition of the planet body. This is the case of super-Earth planets, which are the subject of the present investigation. The gravitational potential of the planet at the distance r from its centre is given by (e.g. Beutler 2005, p. 102)

$$U_{22} = 3\frac{GmR^2}{r^3}C_{22}\cos 2(f - \theta),\tag{1}$$

where G is the gravitational constant and the angles[1] f and θ are as defined in Fig. 1. Note that $\dot{\theta} = \Omega$ is the angular rotation velocity of the planet. The parameter C_{22} describes the equatorial ellipticity of the planet's gravity field and is related to the principal momenta of inertia A, B, C through $C_{22} = (\xi/4)(B - A)/C$, where ξ is the

---

[1] We choose the pericentre of the planet orbit as the origin for the calculation of the longitudes because the main contribution to the variation of the longitude of the pericentre comes from the zonal term proportional to J_2, which has not been included in the present paper (see Ferraz-Mello et al. 2008).
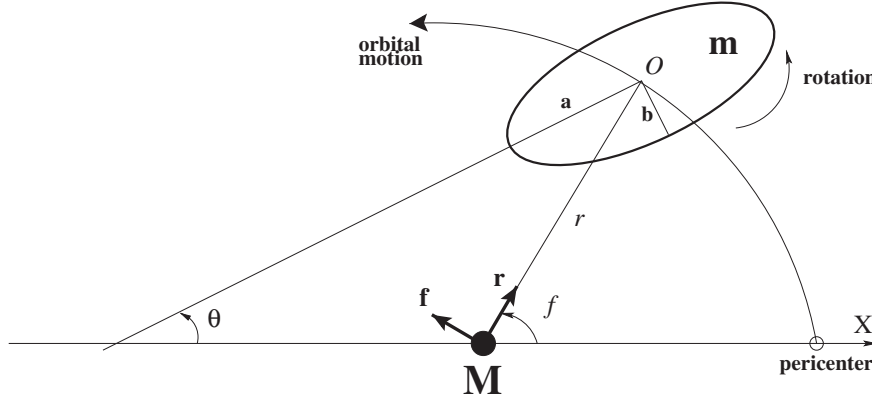
Figure 1. Schematic view of the ellipsoid, showing the angles used in the formulation of the problem. The long axis makes an angle θ with the reference axis X, which is assumed coincident with the orbital pericentre direction. The angle between the long axis and the star–planet direction is given by $f - \theta$, where f is the true anomaly of the planet.

structure constant given by $\xi = C/(mR^2)$ and C is the polar moment of inertia.

We neglect the contribution of terms arising from the oblateness of the rotating body, that is, J_2 and higher order terms. In fact, in the planar problem, the gravitational potential corresponding to the J_2-term depends only on the distance r. In this case, the potential generates a radial force with zero torque that does not affect the rotation evolution.

At the distance r from the centre of the planet, the gravitational field U_{22} gives rise to a force on a point mass M which is given by[2]

$$\boldsymbol{F}_{22} = M \, \nabla U_{22} = M \frac{\partial U_{22}}{\partial r} \, \hat{\boldsymbol{r}} + \frac{M}{r} \frac{\partial U_{22}}{\partial f} \, \hat{\boldsymbol{f}}, \qquad (2)$$

where $\hat{\boldsymbol{r}}$ and $\hat{\boldsymbol{f}}$ are unit vectors with origin in the star (see Fig. 1). The force $\boldsymbol{F}_{22}$ alters the orbital component of the angular momentum, whereas the reaction force governs the evolution of the spin through the creation of the torque on the planet given by $\boldsymbol{T}_{22} = -\boldsymbol{r} \times \boldsymbol{F}_{22} = -M(\partial U_{22}/\partial f)\hat{\boldsymbol{k}}$, where $\boldsymbol{r} = r \, \hat{\boldsymbol{r}}$ and $\hat{\boldsymbol{k}} = \hat{\boldsymbol{r}} \times \hat{\boldsymbol{f}}$. Thus,

$$\boldsymbol{T}_{22} = 6 \frac{GmMR^2}{r^3} C_{22} \sin 2(f - \theta)\hat{\boldsymbol{k}}. \qquad (3)$$

Note that, for $C \dot{\Omega} = T_{22}$ and $C_{22} = (\xi/4)(B - A)/C$, the above equation agrees with the classical expression for the torque (e.g. Danby 1962; Goldreich & Peale 1966).

The effects of the dynamical tides are raised by the gravitational action of the star on the inelastically deformed rotating planet. Due to the internal viscosity of the body, there exists a delay Δt (time lag) between the star perturbation and the maximum deformation. The relationship between Δt and tidal frequencies (which are linear combinations of Ω and n) depends on the internal rheology, which is poorly known even for Solar system bodies. For the sake of simplicity, in this work, we adopt a linear model with constant Δt (Darwin 1880; Mignard 1979; Hut 1981; Rodríguez et al. 2011a); for a review of other tidal models, the reader is referred to Efroimsky & Williams (2009) and Ferraz-Mello (2012).

According to Mignard (1979), the tidal force and torque are given by

$$\boldsymbol{F}_{\text{tide}} = -3k_2 \Delta t \frac{GM^2R^5}{r^{10}}[2\boldsymbol{r}(\boldsymbol{r} \cdot \boldsymbol{v}) + r^2(\boldsymbol{r} \times \boldsymbol{\Omega} + \boldsymbol{v})], \qquad (4)$$

and

$$\boldsymbol{T}_{\text{tide}} = 3k_2 \Delta t \frac{GM^2R^5}{r^8}[-r^2\boldsymbol{\Omega} + \boldsymbol{r} \times \boldsymbol{v}], \qquad (5)$$

where $\boldsymbol{v} = \dot{\boldsymbol{r}}$ and k_2 is the second degree Love number. In this paper, we only consider the tides raised by the star on the planet, neglecting the tides raised on the star by the planet. Indeed, the strength of stellar tide is proportional to the planet mass and can be safely neglected in the case of super-Earths (see Rodríguez & Ferraz-Mello 2010). Note, however, that after circularization of the planet orbit, stellar tides may be the only source of orbital decay.

In the reference frame centred in the star (see Fig. 1), the exact equations of motion of the planet can be now written as

$$\ddot{\boldsymbol{r}} = -\frac{G(M + m)}{r^3}\boldsymbol{r} + \frac{(M + m)}{Mm}(\boldsymbol{F}_{\text{tide}} + \boldsymbol{F}_{22}),$$

$$\ddot{\theta} = \dot{\Omega} = \frac{1}{C}(T_{\text{tide}} + T_{22}). \qquad (6)$$

The perturbing forces $\boldsymbol{F}_{22}$ and $\boldsymbol{F}_{\text{tide}}$ alter the Keplerian orbit of the planet which is defined by the first term of the first equation, while the corresponding torques in the second equation produce variations in the planet rotation. Note that, in the planar case, this last equation can be written in scalar form, because both torques are normal to the orbital plane.

3 NUMERICAL SIMULATIONS

In this section we apply the analytical model described in the previous section in order to investigate the motion of three known super-Earths planets, namely Kepler-10 b, 55 Cnc e and GJ 3634 b. For this task, the exact equations of motion (6) were integrated numerically using the RA15 code (Everhart 1985). We stress that no scaling parameter, often used to accelerate the tidal evolution, was used in our simulations (see e.g. Tittemore & Wisdom 1988 for the validity of the usage of the scaling parameter).

Table 1 shows the physical parameters and current orbital elements of the systems considered in this paper.

3.1 Setting initial configurations

Numerical integrations require a setting of the initial configurations of the systems. In the case of problems including dissipative processes, the choice is complicated, mainly, due to the inadequacy of the simulations of the past evolution of dissipative systems

---

[2] Since we use the expression for U_{22} adopted in Beutler (2005), the corresponding force is computed as the positive gradient of the potential.

Table 1. Physical parameters and current orbital elements of the analysed systems ([a]Batalha et al. 2011; [b]Gillon et al. 2012; [c]Bonfils et al. 2011). The first two planets were discovered through the transit technique, allowing us a good estimation of their radii. $m_\oplus$ and $R_\oplus$ stand for mass and radius of the Earth, respectively.

System	$M(\mathrm{m}_\odot)$	$m(m_\oplus)$	$R(R_\oplus)$	a_{current} (au)	e_{current}
Kepler-10[a]	0.895	4.56	1.416	0.01684	0
55 Cnc[b]	0.905	8.63	2.17	0.0156	0.057
GJ 3634[c]	0.45	7.0	–	0.0287	0.08

through integrations backward in time (see details in Michtchenko & Rodríguez 2011). However, as shown in that paper, the final state of a migrating system is independent of its initial position in the phase space, defined by three values of parameters: the mass and semi-major axes ratios and the total angular momentum. As a consequence, to assess the orbit configuration in the past, we have to set solely the starting semi-major axis value. The initial eccentricity should satisfy the conservation of the total angular momentum of the system.

The total angular momentum of the system is composed of the orbital component written as $m\sqrt{G(M+m)}\sqrt{a(1-e^2)}$, and the rotational component given by $C\Omega = \xi m R^2 \Omega$. Using Kepler's third law, it is easy to show that the ratio of rotational and orbital components is of the order of $(R/a)^2$ (see Rodríguez et al. 2011a); since $R \ll a$, the contribution of rotation to the total angular momentum can be neglected. Therefore, considering that the orbital angular momentum is nearly conserved during tidal migration, we obtain that

$$e_{\mathrm{ini}} \simeq \sqrt{1 - \frac{a_{\mathrm{current}}}{a_{\mathrm{ini}}}(1 - e_{\mathrm{current}}^2)}, \tag{7}$$

where the subscripts 'ini' and 'current' stand for initial and current orbital elements, respectively. In this way, choosing an initial value for the semi-major axis and knowing the current values of a and e, equation (7) allows us to constrain the initial value of the eccentricity (see the next section and specially Fig. 6). It should be emphasized that the value obtained in such a way must be considered as an approximation of the initial value of the eccentricity, since the planets may belong to systems with two or more planets.

The value of Δt is determined by the relationship between the tidal frequency ν and the quality factor Q. In the case of a linear approximation, we have $1/Q = \nu \Delta t$, where $\Delta t = $const. It is known that, in the Fourier spectrum of the tidal potential, the most important frequencies (i.e. those involved in terms of order zero and order one in the eccentricity) are $\nu_0 = 2\Omega - 2n$, $\nu_1 = 2\Omega - 3n$ and $\nu_2 = 2\Omega - n$. The first one is associated with the term which is independent of the eccentricity, while the two last frequencies correspond to terms which are proportional to e (Darwin 1880; Ferraz-Mello et al. 2008). Using the frequency ν_0 and a modified version of the quality factor written in terms of the Love number k_2 as $Q' = 3Q/2k_2$, we obtain

$$k_2 \Delta t = \frac{3}{4Q'(\Omega - n)}. \tag{8}$$

Actually, the spin rotation of exoplanets is not available from observations, thus we choose its initial value arbitrarily but considering a super-synchronous motion ($\Omega > n$).

Finally, according to Callegari & Rodríguez (2012), the equilibrium shape attained by the planet due to the gravitational interaction with the star results in a prolateness, or equatorial ellipticity, which can be computed as $(B - A)/C \simeq (15/4)(M/m)(R/r)^3$. Knowing that

$C_{22} = (\xi/4)(B - A)/C$ we can obtain the magnitude of C_{22} for the planets with estimated radius. For the planets Kepler-10 b and 55 Cnc e (see Sections 3.2.1 and 3.2.3), we obtain $C_{22} \simeq 10^{-3}$ and $C_{22} \simeq 2.4 \times 10^{-3}$, respectively, assuming $r = a_{\mathrm{current}}$. For the sake of comparison with some rocky Solar system tidally evolved bodies, we note that $C_{22} = 8.1 \times 10^{-6}$ in the case of Mercury (Smith et al. 2012), $C_{22} = 1.0 \times 10^{-5}$ for Titan (Iess et al. 2010) and $C_{22} = 5.6 \times 10^{-4}$ for Io (Schubert et al. 2004).

3.2 Results

The integration of the exact equations of motion usually requires a long computation time. For this reason, we decided to work with a small set of initial spin–orbit configurations and physical parameters. A statistical analysis taking into account many different initial conditions could give us a more accurate global picture of the past spin–orbit evolution of the planets. As pointed out by Correia & Laskar (2009), such statistical study is more adequate in the context of the averaged equations of the spin–orbit problem (see Section 4).

3.2.1 Kepler-10 b

Kepler-10 b is a very close-in planet with a period of ∼0.84 d, orbiting an old (≃12 Gyr) Sun-like star (Batalha et al. 2011). The physical parameters and the current orbital elements of the planet are summarized in Table 1. The estimated mass and radius values ($m = 4.56 m_\oplus$, $R = 1.416 R_\oplus$) suggest a rocky composition of the planet, which can be considered as a super-Earth (Valencia 2011). The transit technique measurements do not allow a reliable estimation of the current orbital eccentricity, which was arbitrarily fixed at zero in this work. This choice is supported by our numerical simulations of the whole system, which includes also the exterior companion, Kepler-10 c. The results have shown that the long-term evolution, due to the coupled effect of tides and mutual interaction, could result in the complete circularization of both planetary orbits.

We adopt the initial semi-major axis at $a_{\mathrm{ini}} = 0.02$ au, which provides $e_{\mathrm{ini}} = 0.397$ through equation (7). In addition, we set $\Omega_{\mathrm{ini}} = 2.7 n_{\mathrm{ini}}$ and $\xi = 0.35$. For the tidal parameter, we assume $Q' = 100$ (a value usually adopted for rocky planets) and, solving equation (8), we obtain $k_2 \Delta t \simeq 1.1$ min.

In Section 3.1 we have estimated that, for Kepler-10 b on its current orbit, $C_{22} \simeq 10^{-3}$. It should be emphasized that C_{22} would be smaller if the frozen-in shape of the planet was attained at larger distances than a_{current}. Hence, in order to investigate different possible scenarios, we consider three different values of C_{22}, namely 10^{-3}, 10^{-4} and 10^{-5}.

Fig. 2 shows the variation in Ω/n as a function of the eccentricity of Kepler-10 b. The curve with segments line corresponds to the stationary tidal solution (STS) of the rotation ($\dot{\Omega} = 0$), obtained when only the tidal torque is considered. The STS is a function which depends only on the planet eccentricity,[3] and is given by

$$\Omega_{\mathrm{stat}}/n = 1 + 6e^2 + 3e^4/8 + 223e^6/8 + \mathcal{O}(e^7) \tag{9}$$

(see equations 42 or 43 of Hut 1981; see also Section 4 for more details). The stationary rotation evolves with the tidally damped eccentricity and the system reaches synchronization ($\Omega = n$) only for circular orbits. Note that for small values of e, there follows that

---

[3] It is worth noting that the STS does not depend on any physical parameter of the interacting bodies. However, alternative tidal theories show that the STS would depend on the internal viscosity (see Ferraz-Mello 2012).
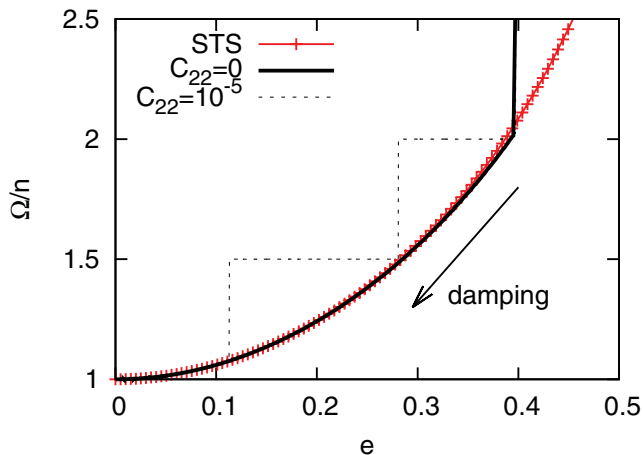
Figure 2. The variation of the rotation with eccentricity of the Kepler-10 b orbit. The arrow indicates the direction of the eccentricity and rotation evolutions. The curve with segment line shows the STS of the rotation, indicating a good agreement with the result of numerical simulation for $C_{22} = 0$ (solid black curve). The dotted line corresponds to the case $C_{22} = 10^{-5}$, where the trappings 2/1 and 3/2 occur. After escaping from the 3/2 resonant motion, the rotation follows the STS towards a synchronization between the rotation and orbital motions.

$\Omega \sim n$; for this reason, the STS is also called the pseudo-synchronous solution (but this is valid only for $e \ll 1$).

The solid black curve in Fig. 2 corresponds to the result of the numerical simulation performed with $C_{22} = 0$ (only tidal forces are considered). In this case, the stationary rotation is attained almost instantaneously (when compared to the time of circularization). Note that both curves are in good agreement, at least for $e < 0.4$; hence, in this eccentricity interval, we can refer to the solution obtained with $C_{22} = 0$ as STS. We also note that the curve for $C_{22} = 0$ reaches the STS for Ω/n close to two; however, this is incidental and unrelated with the 2/1 trapping.

Fig. 3 shows the time variation of Ω/n. For the three considered values of $C_{22} > 0$, the rotation rapidly encounters the value $\Omega/n = 2$ and thus the planet rotation is captured in the 2/1 SOR. On one
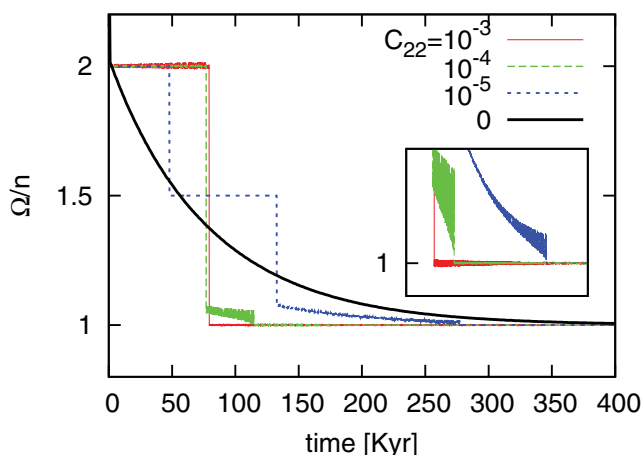
Figure 3. Time variation of the ratio Ω/n for Kepler-10 b depending on the value of C_{22}. Different evolutions are observed, including captures in 2/1, 3/2 and 1/1 SORs. The solid black curve corresponds to the evolution for $C_{22} = 0$ (i.e. when only the tidal torque exist) and coincides with the STS (see the text for discussion) of the rotation. The captures in the synchronous motion are detailed on the small panel.

hand, for $C_{22} = 10^{-3}$ and $C_{22} = 10^{-4}$, the rotation escapes from the 2/1 trapping approximately at 80 Kyr, when the rotation drops to the value $\Omega/n = 1$, implying capture into 1/1 SOR and synchronous motion. However, it is worth noting that, for $C_{22} = 10^{-3}$, the synchronism is attained in a form of jump, whereas for $C_{22} = 10^{-4}$ the rotation evolves without capture for a very short time before the 1/1 SOR (see small panel in Fig. 3). We have also plotted the result for $C_{22} = 0$, showing that synchronization is attained around 400 Kyr. It is interesting to note that the introduction of the equatorial asymmetry of the planet reduces the time to reach synchronization; for instance, for $C_{22} = 10^{-3}$, it is reduced by a factor of 5.

On the other hand, when $C_{22} = 10^{-5}$, the 2/1 SOR is destabilized at around 48 Kyr giving rise to the trapping in the 3/2 SOR ($\Omega/n = 3/2$). Thus, the permanence of the rotation in the 2/1 SOR is temporary and its duration clearly depends on the C_{22} value. The rotation evolves in a Mercury-like state for some time, when a new instability occurs, after which an evolution free of trapping starts. Note that during the period of non-capture, the rotation returns to the stationary value, as can be seen in the dotted curve of Fig. 2 when $e \leq 0.11$. Finally, the synchronization is reached at around 270 Kyr.

Figs 4 and 5 show the time evolution of semi-major axis and eccentricity of Kepler-10 b. We note that, when the rotation evolves under capture in resonance (i.e. for $C_{22} > 0$), the rates of variations of the elements are larger than the one corresponding to the pure tidal case ($C_{22} = 0$), with the difference increasing as the eccentricity is damped (when the comparison is done for a given SOR). Moreover, for the same value of C_{22}, the rate of orbital decay and circularization seems to depend on the specific SOR in which the planet rotation is trapped in. For example, in the case of $C_{22} = 10^{-5}$, the evolutions of a and e show two different regimes as the rotation evolves first in the 2/1 and then in 3/2 trappings (see Section 4).

We note that the time necessary to get an orbit with $e = 0.05$ is much greater for $C_{22} < 10^{-3}$. In fact, when the rotation evolves without capture, the time-scale for circularization increases, according to Figs 4 and 5.

It is worth noting that, in the case of $C_{22} > 0$, the synchronous motion can be attained even for $e \neq 0$. For instance, in the case of $C_{22} = 10^{-4}$, the system is captured in 1/1 SOR at roughly 120 Kyr, when $e \simeq 0.079$. This fact confirms the classical result that, for eccentric orbits, the synchronous motion is only possible if there exists an additional torque which counteracts the tidal torque (see Goldreich & Peale 1966; Ferraz-Mello et al. 2008 and references therein). We also note that after circularization, the 1/1 SOR is the only possible resonant motion.[4]

Fig. 6 shows the evolution of the system in the plane of orbital elements a and e. The solid line shows the result of numerical simulation in the case of $C_{22} = 10^{-3}$. The dashed line corresponds to equation (7), which is independent of the value of C_{22}. Note as both curves are in very good agreement, in such a way confirming our assumption about the conservation of the orbital angular momentum (Section 3.1).

3.2.2 GJ 3634 b

GJ 3634 b is a super-Earth planet with mass $m = 7.0 m_{\oplus}$ orbiting an M2.5 dwarf every 2.65 d with an eccentricity of $e = 0.08$ (Bonfils

---

[4] Except if an additional mechanism, such as impact events, acts to destabilize the synchronous motion (see Correia & Laskar 2012; Wieczorek et al. 2012).
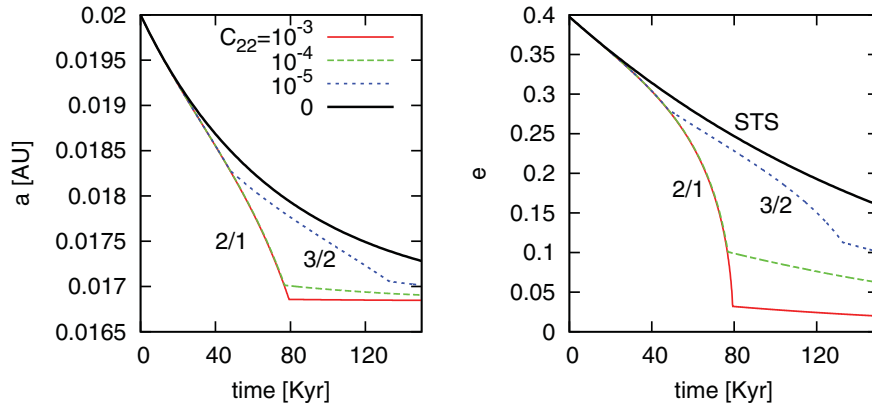
Figure 4. Time variation of semi-major axis (left-hand panel) and eccentricity (right-hand panel) of Kepler-10 b along the first 150 Kyr of evolution. The variation rates of a and e depend on the specific capture in which the rotation is trapped in. As different values of C_{22} lead to several captures, different scenarios are expected for the orbital evolution, despite the final values of the elements being the same for all C_{22} (see the next figure).
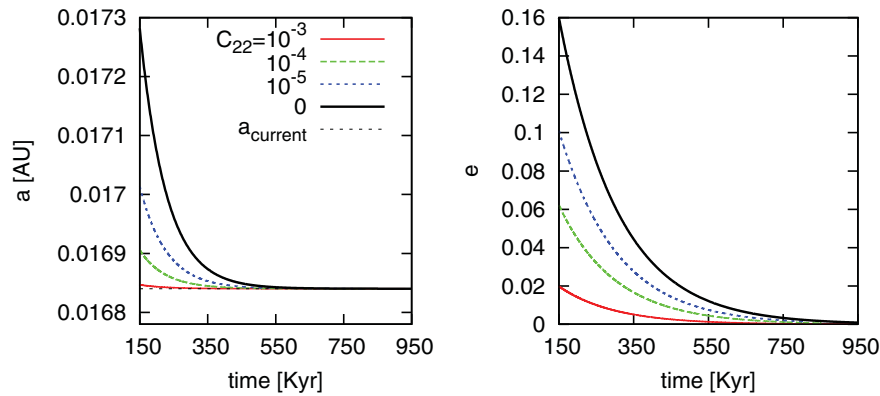
Figure 5. Continuation of Fig. 4 shows the final evolution. The orbital decay continues until circularization is achieved. The current semi-major axis of Kepler-10 b coincides with the one obtained in the simulation.
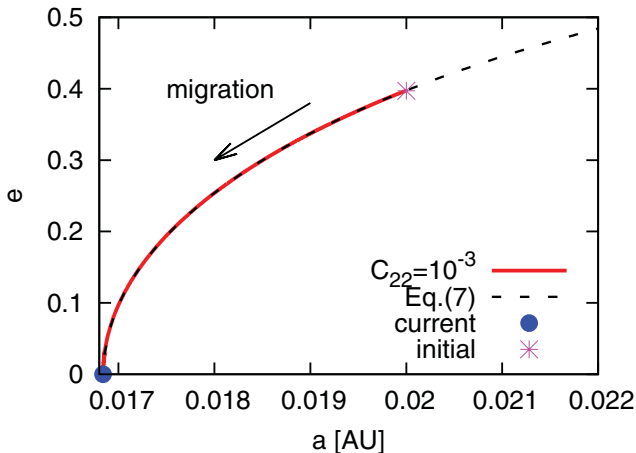
Figure 6. Evolution of the orbit of Kepler-10 b in the plane (a, e). The solution of equation (7) is shown by the dashed line and is compared to the result of the numerical simulation for the case $C_{22} = 10^{-3}$, giving a good agreement [the curves for the other two C_{22} values also agree with the solution of equation (7), but are not shown here for the sake of simplicity]. The starting position of the planet is indicated by the star symbol.

et al. 2011). Since there is no transit detection for this planet, its radius is unknown. However, Valencia, Sasselov & O'Connell (2007) have shown that there is a maximum radius that a rocky terrestrial planet may achieve for a given mass. A larger radius would imply a

large amount of water and even the possibility of a massive volatile envelope. Indeed, for a planet with mass $7.5 m_\oplus$ the maximum terrestrial radius would be 11 600 km ($\simeq 1.82 R_\oplus$), which results in a mean density of $\rho \simeq 1.25 \rho_\oplus$. Hence, we assume for GJ 3634 b that $\rho = \rho_\oplus$ to obtain $R \simeq 1.9 R_\oplus$.

The adopted initial orbital elements are $a_{ini} = 0.033$ au and $e_{ini} = 0.369$, while $\Omega_{ini} = 3.7 n_{ini}$, $\xi = 0.35$ and $Q' = 100$ ($k_2 \Delta t = 2.1$ min). At the current value of the semi-major axis the estimated value of C_{22} is $C_{22} \simeq 1.6 \times 10^{-4}$ (Section 3.1); in this work, we perform the analysis using two values of C_{22}: 10^{-4} and 10^{-5}.

Fig. 7 shows the variation of Ω/n as a function of e (left-hand panel) and the time variation of a (right-hand panel). For $C_{22} = 10^{-4}$, the rotation is rapidly trapped in the 2/1 SOR, remaining in such resonant configuration during most of the time of the tidal eccentricity damping. Only at low eccentricities, close to 0.032, the system leaves the 2/1 SOR dropping directly into the synchronous motion.

At variance, for $C_{22} = 10^{-5}$, the rotation quickly reaches the stationary (non-resonant) state given by the STS curve ($C_{22} = 0$) in Fig. 7 (left). The system evolves along the STS curve up to close approach to the 3/2 SOR. Then, the system is captured and remains in this resonance until dropping in the synchronized state, at $e \simeq 0.012$.

In both cases, the final configuration of the planet's orbit is characterized by circularization and synchronization, as in the case of Kepler-10 b. However, the current eccentricity of GJ 3634 b is different from zero (its location at 0.08 is shown by the dotted vertical
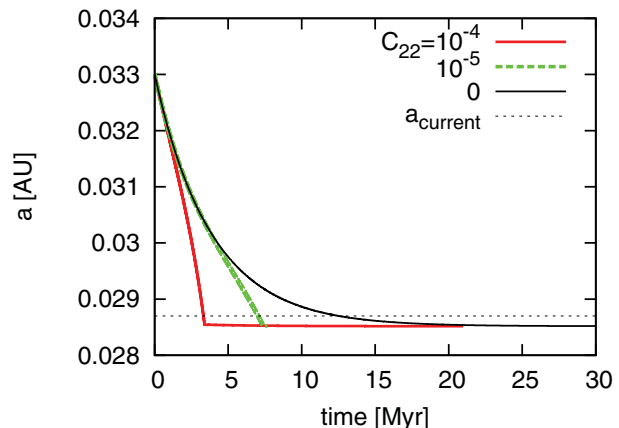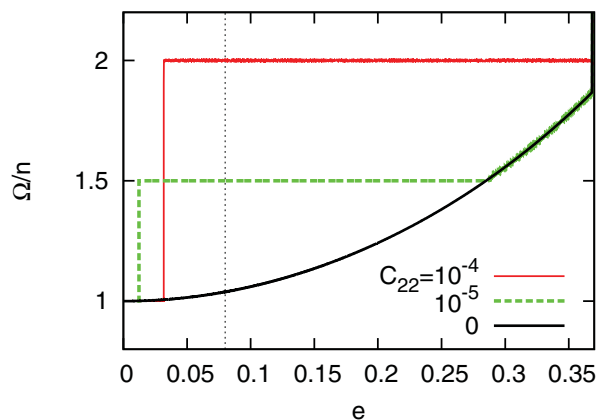
Figure 7. The variation of Ω/n as a function of e (left-hand panel) and the time evolution of a (right-hand panel) for the planet GJ 3634 b. Depending on C_{22}, the planet rotation may be currently evolving in either 2/1 or 3/2 SOR. Note that the time-scale of orbital decay is drastically reduced provided the planet can support a permanent deformation resulting in a non-zero C_{22} value. The vertical and horizontal dotted lines indicate the current values of e and a, respectively.

line in the left-hand panel of Fig. 7). Note that the current eccentricity is reached when the rotation still evolves in the 2/1 or 3/2 SOR (depending on C_{22}). This fact suggests that GJ 3634 b could be presently involved in one of such resonant trappings, in particular, it could be found in a Mercury-like rotational state ($\Omega/n \simeq 3/2$). However, it should be kept in mind that this conclusion depends on the choice of specific values of C_{22} and Q'. Indeed, the results of an additional simulation performed with $C_{22} = 10^{-6}$ have shown that the trapping of the system in the 3/2 SOR is destabilized at $e \simeq 0.11$. Since $e_{\text{current}} = 0.08 < 0.11$, the planet rotation would be currently evolving without capture (along the STS) for such a small C_{22} value.

The semi-major axis evolution (Fig. 7, right-hand panel) shows that the tidal decay is faster when the rotation of the planet is trapped in the 2/1 and 3/2 spin–orbit resonant motions. The fact that the current eccentricity of the planet orbit is different from zero suggests that, in the absence of other perturbations, the orbital decay[5] of the planet is presently in progress and, consequently, the final semi-major axis will be smaller than the current one.

3.2.3 55 Cnc e

55 Cnc e is a hot super-Earth planet, with mass $m = 8.63 m_\oplus$ and radius $R = 2.17 R_\oplus$, orbiting a Sun-like star each 0.74 d with $e = 0.057$ (Winn et al. 2011; Gillon et al. 2012). The averaged density of the planet is comparable to that of the Earth, suggesting a rock–iron composition supplemented by a significant mass of water, gas or other light elements[6] (Winn et al. 2011).

For numerical simulations, we adopt $a_{\text{ini}} = 0.0186$ au, $e_{\text{ini}} = 0.4$, $\Omega_{\text{ini}} = 2.7\,n_{\text{ini}}$ and $\xi = 0.35$. The tidal history of the system indicates that the magnitude of Q' must be higher than the commonly adopted values for rocky planets (Ferraz-Mello 2012). In this work, we use $Q' = 5.5 \times 10^3$; this value allows us to obtain $k_2 \Delta t \simeq 1.1$ s. We perform numerical simulations for two different values of C_{22}: 10^{-3} and 10^{-4}. For the purpose of further comparison with the results reported in Callegari & Rodríguez (2012), we also consider the values $C_{22} = 2.45 \times 10^{-3}$ and 2.45×10^{-4}.

[5] In fact, $\dot{a} \propto e^2$ when $\Omega = n$ or $\Omega \simeq n$ (see equation 20).
[6] The physical composition and the suggested value of Q' (5.5×10^3) indicate that the possibility of 55 Cnc e to be a mini-Neptune instead of a super-Earth should not be ruled out.
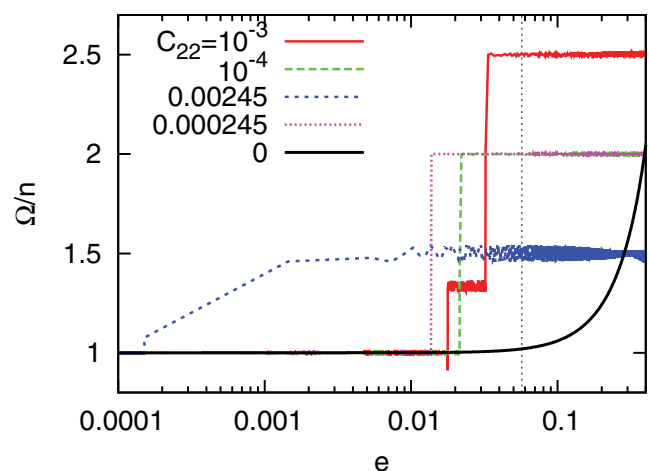

Figure 8. The variation Ω/n as a function of e (in logarithmic scale), for the planet 55 Cnc e. We have used $C_{22} = 10^{-3}$ in addition to the value adopted in Callegari & Rodríguez (2012) $C_{22} = 2.45 \times 10^{-3}$. Also values 10 times smaller were taken into account for the sake of completeness. The vertical dotted line indicates the current value of e, namely 0.057. The trappings in the RSOs 5/2, 2/1, 3/2, 4/3 and 1/1 appear during the evolutions. Note the large amplitude oscillation of Ω/n inside the 3/2 and 4/3 cases with C_{22} of the order of 10^{-3}. Depending on C_{22}, 55 Cnc e can be an example of a planet currently evolving in the 5/2, 2/1 or 3/2 SOR.

Fig. 8 shows the evolution of rotation as a function of the planet's eccentricity. The captures inside the 5/2, 2/1, 3/2, 4/3 and 1/1 resonances can be observed. For $C_{22} = 2.45 \times 10^{-3}$, the planet rotation evolves under capture in the 3/2 SOR almost up to the orbital circularization, with Ω/n roughly varying between 1.46 and 1.54.

In a recent work, Callegari & Rodríguez (2012) have shown that, for $e = 0.057$ and $(B - A)/C = 0.028$ (or $C_{22} = 2.45 \times 10^{-3}$), the phase space of the rotation ($\dot{\theta}/n, \theta$) of 55 Cnc e, between the main SORs, is dominated by a large region of chaotic motion. This region increases as larger values of the eccentricity are considered.

Capture in SOR can work as a mechanism to prevent a chaotic rotation, provided that the dissipation is large enough in order to ensure the corresponding trapping. According to our simulations (see Fig. 8), destabilizations of different resonances occur as the eccentricity is tidally damped (see also the next section), giving rise to new temporary trappings with a subsequent evolution to
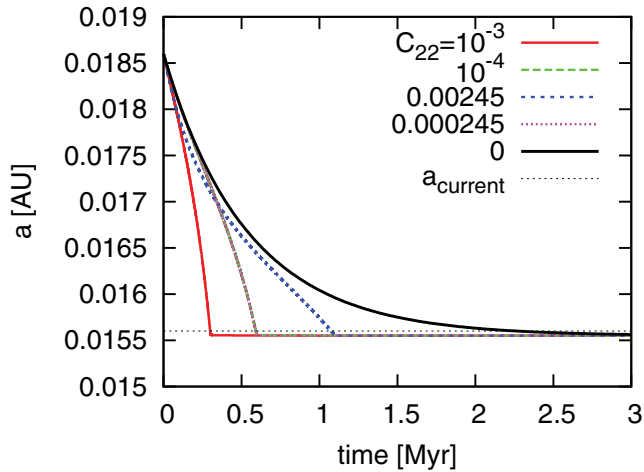
Figure 9. Time variation of semi-major axis for 55 Cnc e. The curves show the evolution for four values of C_{22} together with the STS curve. As for previously analysed planets, the orbital decay is faster when the planet rotation is trapped in a resonant motion. The current value of a is obtained for all values of C_{22}.

synchronism. In this way, a chaotic behaviour of the rotation can be avoided by a continuous evolution under a resonant motion. It is important to note that, at least for the cases shown in Fig. 8, there is no interval of non-resonant motion between two successive trappings, as in the case of Kepler-10 b (see Fig. 3 for $C_{22} = 10^{-4}$ and 10^{-5}).

An additional simulation done with $C_{22} = 2.45 \times 10^{-5}$ (not shown in figures) has resulted in a 2/1 trapping until $e \simeq 0.04$, indicating that the planet rotation may be currently evolving in resonant motion for such a small value of C_{22}.

Fig. 9 shows the time variation of the semi-major axis. It is worth noting that the orbital decay results in a more rapid evolution towards $a_{current}$ when the planet rotation is trapped in a SOR. Also, the rate of variation depends on the specific resonance. From Fig. 9 we see that the evolution when $C_{22} \sim 10^{-4}$ (capture in 2/1) is almost two times faster than the one for $C_{22} = 2.45 \times 10^{-3}$ (3/2 capture). We will return to this discussion in the next section.

4 AVERAGED EQUATIONS

In order to better understand the results previously obtained through numerical simulations of the exact equations of motion, in this section, we develop an analytical approach in the context of the averaged equations of the spin–orbit problem.

The equation of motion for the spin in equation (6) cannot be solved analytically. However, because we are interested in the evolution inside SORs, we will consider planetary spin rates having values such that $\Omega \simeq pn$, where p is a half-integer. Our investigation is restricted to the cases $p = 1$, $p = 3/2$ and $p = 2$ but can be easily extended to any other SOR.

We introduce the 'resonant' angle $\delta = \theta - p\, l$, where l is the mean anomaly of the planet orbit and θ is as defined in Section 2. Note that the angle δ gives the orientation of the long axis whenever the planet passes through the pericentre of its orbit (i.e. $\delta = \theta$ when $l = 0$; see Fig. 1). It is easy to show that, inside the SOR given by the parameter p, the resonant angle is a slowly varying variable when compared to the orbital period of the planet. Indeed, we can write that $\dot\theta = \dot\delta + pn$, where $\dot\theta = \Omega \simeq pn$ and, consequently, $\dot\delta \simeq 0$. Now, replacing θ by $\delta + pl$ in equation (3) and averaging over the

orbital period, we obtain the classical result for the averaged torque on the planet produced by the permanent equatorial deformation (see Goldreich 1966; Goldreich & Peale 1966):

$$\langle T_{22}\rangle = -6mR^2 C_{22} n^2 H(p, e)\sin 2\delta, \tag{10}$$

where $H(p, e)$ are power series of e with the leading term of order $e^{2|p\,-1|}$ (see Appendix A for a literal expansion up to the seventh order).

The averaged tidal torque on the planet is given by

$$\langle T_{tide}\rangle = K_{tide}\left(\frac{n}{a}\right)^3 \mathcal{T}(p, e), \tag{11}$$

where $K_{tide} = 3k_2 \Delta t M R^5$ and $\mathcal{T}(p, e)$ is a suitable function, whose expansion in powers of e is shown in Appendix A (Hut 1981).

At resonance, the equilibrium solution of the rotation is given by the condition

$$C\dot\Omega = \langle T_{tide}\rangle + \langle T_{22}\rangle = 0, \tag{12}$$

and, resolving for $C_{22}\sin 2\delta$, we obtain

$$C_{22}\sin 2\delta = \frac{1}{2}k_2 \Delta t\, n\frac{M}{m}\left(\frac{R}{a}\right)^3 \frac{\mathcal{T}(p, e)}{H(p, e)}. \tag{13}$$

If we know the maximum value that δ can reach without disturbing the trapping in the p-SOR, we may obtain the minimum value of C_{22} necessary for capture in the same resonant motion.

4.1 1/1 spin–orbit resonance

Replacing $p = 1$ in equation (13) and expanding the ratio $\frac{\mathcal{T}(p,e)}{H(p,e)}$ in powers of e, up to the order of 6, we obtain

$$C_{22}\sin 2\delta = \frac{1}{16}k_2 \Delta t\, n\frac{M}{m}\left(\frac{R}{a}\right)^3$$
$$\times (48e^2 + 483e^4 + 2624e^6) + \mathcal{O}(e^8). \tag{14}$$

We note that, for $\mathcal{O}(e^4)$, the above expression is obtained in the same way as in Ferraz-Mello et al. (2008) for synchronous asymmetric planets.[7]

4.1.1 Semi-major axis evolution

The averaged variation of the orbital elements can be obtained using the Euler–Gauss equations (see Beutler 2005, p. 230), which are written in terms of the radial and transverse components of the perturbing force. The result for the semi-major axis is

$$\langle \dot a_{22}\rangle = -\frac{3nR^2 C_{22}\sin 2\delta}{72a}\left(-288 + 720e^2 - 234e^4 + 35e^6\right) + \mathcal{O}(e^8). \tag{15}$$

Replacing $C_{22}\sin 2\delta$ by the corresponding expression given in equation (14), we obtain

$$\langle \dot a_{22}\rangle = 3k_2 \Delta t\frac{M}{m}\left(\frac{R}{a}\right)^5 n^2 a\left(12e^2 + \frac{363}{4}e^4 + \frac{2911}{8}e^6\right) + \mathcal{O}(e^8). \tag{16}$$

In the context of the linear tidal model, the averaged variation of the semi-major axis due to tides is given by equation (9) of Hut

---

[7] In this case, the association $\epsilon_2 = (2\Omega - n)\Delta t = n\Delta t$ should be done, where ϵ_2 is the phase lag of the tidal wave whose frequency is $(2\Omega - n)$.

(1981), valid for any values of p and e. The expansion up to $\mathcal{O}(e^8)$ reads

$$\langle \dot{a}_{\text{tide}} \rangle = 3k_2 \Delta t \frac{M}{m} \left(\frac{R}{a} \right)^5 n^2 a \Big[2(-1+p) + (-46+27p)e^2$$

$$+ \frac{3}{4}(-480+191p)e^4 + \frac{1}{8}(-13530+3961p)e^6 \Big] + \mathcal{O}(e^8). \quad (17)$$

Replacing $p = 1$ in the above equation we obtain

$$\langle \dot{a}_{\text{tide}} \rangle_{p=1} = -3k_2 \Delta t \frac{M}{m} \left(\frac{R}{a} \right)^5$$

$$\times n^2 a \left(19e^2 + \frac{867}{4}e^4 + \frac{9569}{8}e^6 \right) + \mathcal{O}(e^8). \quad (18)$$

The total averaged variation of the semi-major axis is then given as

$$\langle \dot{a} \rangle_{p=1} = \langle \dot{a}_{\text{tide}} \rangle_{p=1} + \langle \dot{a}_{22} \rangle \quad (19)$$

and thus

$$\langle \dot{a} \rangle_{p=1} = -3k_2 \Delta t \frac{M}{m} \left(\frac{R}{a} \right)^5$$

$$\times n^2 a \left(7e^2 + \frac{504}{4}e^4 + \frac{3329}{4}e^6 \right) + \mathcal{O}(e^8). \quad (20)$$

At the same order of approximation, the above equation coincides with the result of previous works (see Ferraz-Mello et al. 2008, and references therein).

When only the tidal torque on the planet is taken into account, the non-resonant STS is given by equation (9). In this case, the synchronism is possible only for circular orbits. If instead of $p = 1$, we replace $p = p_{\text{stat}} = \Omega_{\text{stat}}/n$ in equation (17), we obtain

$$\langle \dot{a}_{\text{tide}} \rangle_{p=p_{\text{stat}}} = -3k_2 \Delta t \frac{M}{m} \left(\frac{R}{a} \right)^5$$

$$\times n^2 a \left(7e^2 + 54e^4 + \frac{1133}{4}e^6 \right) + \mathcal{O}(e^8). \quad (21)$$

We define r_a^p as the ratio between averaged semi-major axis variation in the p-SOR ($p = 1, 3/2, 2, \ldots$) and in the tidal stationary solution of the rotation ($p = p_{\text{stat}}$), that is

$$r_a^p \equiv \frac{\langle \dot{a} \rangle_p}{\langle \dot{a}_{\text{tide}} \rangle_{p=p_{\text{stat}}}}. \quad (22)$$

Comparing equations (20) and (21), we note that $r_a^{p=1} > 1$, indicating that the rate of semi-major axis decay is stronger when the rotation is locked in the 1/1 SOR, compared to the case when it evolves following the STS. This result is in agreement with Wisdom (2008), who has shown that the rate of energy dissipation in a body with synchronous rotation is larger than in an asymptotic non-synchronous rotation.

4.1.2 Eccentricity

We repeat the procedure described in the previous section to obtain the averaged variation of the planet eccentricity. The resulting expressions are

$$\langle \dot{e}_{22} \rangle = -9k_2 \Delta t \frac{M}{m} \left(\frac{R}{a} \right)^5 n^2 \left(e^3 + \frac{117}{16}e^5 \right) + \mathcal{O}(e^7), \quad (23)$$

$$\langle \dot{e}_{\text{tide}} \rangle_{p=1} = -\frac{3}{2}k_2 \Delta t \frac{M}{m} \left(\frac{R}{a} \right)^5$$

$$\times n^2 \left(7e + 113e^3 + \frac{5299}{8}e^5 \right) + \mathcal{O}(e^7), \quad (24)$$
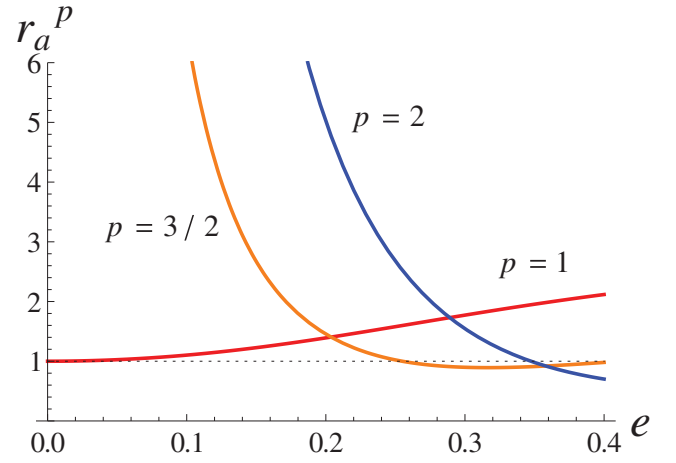
Figure 10. The variation of r_a^p as a function of orbital eccentricity, for $p = 2, 3/2$ and 1. In the cases of $p > 1$ the ratio of rates of variation of a in the SOR and in the STS increases for small e, showing that the orbital decay is enhanced (when compared with the evolution in the STS) whenever the planet rotation evolves under resonance with the orbital motion.

$$\langle \dot{e}_{\text{tide}} \rangle_{p=p_{\text{stat}}} = -\frac{3}{8}k_2 \Delta t \frac{M}{m} \left(\frac{R}{a} \right)^5$$

$$\times n^2(28e + 188e^3 + 917e^5) + \mathcal{O}(e^7), \quad (25)$$

$$\langle \dot{e} \rangle_{p=1} = -\frac{3}{8}k_2 \Delta t \frac{M}{m} \left(\frac{R}{a} \right)^5 n^2(28e + 476e^3 + 2825e^5) + \mathcal{O}(e^7). \quad (26)$$

Similarly to the semi-major axis variation case, $r_e^{p=1} > 1$, where r_e^p is the analogous for the eccentricity of equation (22).

4.2 3/2 and 2/1 spin–orbit resonances

We analyse in this section the spin–orbit behaviour when the planet evolves in the 3/2 and 2/1 SORs, employing the same method described in the previous section.[8] We have

$$\langle \dot{a} \rangle_{p=3/2} = -3k_2 \Delta t \frac{M}{m} \left(\frac{R}{a} \right)^5$$

$$\times n^2 a \left(\frac{1}{2} - \frac{5}{4}e^2 + \frac{774}{16}e^4 + \frac{8019}{16}e^6 \right) + \mathcal{O}(e^8), \quad (27)$$

and

$$\langle \dot{a} \rangle_{p=2} = -3k_2 \Delta t \frac{M}{m} \left(\frac{R}{a} \right)^5 n^2 a \left(2 - 2e^2 - 3e^4 + \frac{943}{4}e^6 \right) + \mathcal{O}(e^8). \quad (28)$$

Fig. 10 shows a plot of r_a^p for the three analysed resonances as a function of the eccentricity. On the one hand, we note that $r_a^{p=3/2}$ and $r_a^{p=2}$ increase for small eccentricity, indicating that the major effect on the orbital evolution due to the resonance captures occurs as e decreases, in agreement with the results of the numerical simulations (see Figs 4, 7 and 9). On the other hand, for large e, r_a is small (mainly in the case $p = 3/2$) as also shown in Figs 4 and 7, where there is a small difference between the evolutions with and without C_{22} (i.e. $r_a \simeq 1$).

---

[8] We stress that $H(p > 1, e)$ has no term independent of e and thus equation (13) cannot be expanded around $e \simeq 0$.
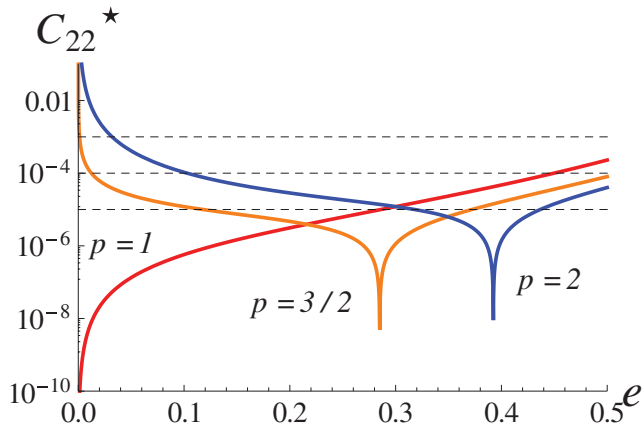
Figure 11. Critical value of C_{22} given by equation (13) and calculated with parameters of the planet Kepler-10 b. The calculation of C_{22}^* can be used as a guide to investigate the stability of a given SOR as a function of eccentricity (see the text for discussion). Note that in the case of $p = 1$ we have $C_{22}^* = 0$ for $e = 0$ (see equation 14), indicating that the synchronism is the only possible resonant motion for circular orbits (see Goldreich & Peale 1966; Celletti & Chierchia 2008; Callegari & Rodríguez 2012).

When the synchronous motion is analysed, we note in Fig. 10 that $r_a^{p=1}$ is an increasing function of e, indicating that the orbital decay when the rotation is trapped in the 1/1 SOR is large for large e. However, as simulations show, synchronism is attained for very low values of e, making the orbital decay almost negligible.

The results above are also valid for r_e^p. It is interesting to note that r_a^p and r_e^p are only functions of the eccentricity and do not depend on any physical parameter.

It is worthwhile to mention that T_{22} averages to zero unless the condition $\Omega \simeq pn$ is assumed (whit p integer), that is, the averaged orbital evolution due to the triaxial torque is expected only for resonant cases.

4.3 Critical C_{22}

As has been noted, equation (13) can be used to obtain the minimum value of C_{22} necessary for the stability of the p-SOR. Calling C_{22}^* the one value given by the right-hand side of equation (13), the stability condition for a resonant spin state requires that $C_{22} > C_{22}^*$. The above condition is frequently found in the literature as strength criterion of the resonance (see Murray & Dermott 1999, p. 205).

Fig. 11 shows the functional dependence of the absolute value of C_{22}^* with the eccentricity, obtained for Kepler-10 b. The dashed horizontal lines represent three values of C_{22} used in the numerical simulations shown in Section 3.2.1, namely 10^{-3}, 10^{-4} and 10^{-5}.

The case $p = 2$, shown by the blue curve, indicates that $C_{22}^* = 10^{-5}$ for $e \simeq 0.3$, $C_{22}^* = 10^{-4}$ for $e \simeq 0.1$ and $C_{22}^* = 10^{-3}$ for $e \simeq 0.03$. A good agreement is obtained doing the comparison with the results of the numerical simulations for Kepler-10 b, shown in Fig. 12. Note that the 2/1 SOR destabilizes when $e \simeq 0.28$, $e \simeq 0.1$ and $e \simeq 0.03$.

The same can be observed for the 3/2 SOR, in which the rotation escapes from the trapping when $e \simeq 0.11$ if $C_{22} = 10^{-5}$, in concordance[9] with the result of Fig. 11 (orange curve).

[9] Small differences between the result of numerical simulations and the analysis of averaged equations may arise because for the construction of Fig. 11 we use $a = a_{\text{current}}$, taking also into account that truncated series in e were used for the same figure.
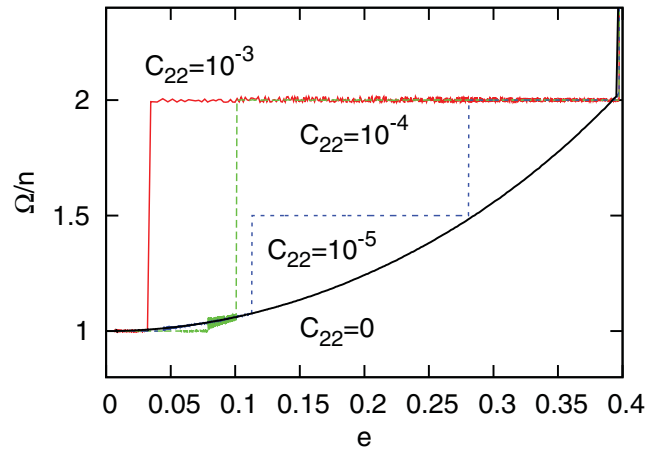
Figure 12. The variation of Ω/n as a function of the orbital eccentricity for Kepler-10 b, resulting from the analysis of numerical simulations of the exact equations of motion (see Section 3.2). If a comparison with the results of Fig. 11 is done, we obtain a good agreement for the values of e for which each SOR destabilizes (see the text for details).

Since for roughly $e \leq 0.1$ the condition $C_{22} > C_{22}^*$ is satisfied more easily for $p = 1$ as compared to $p > 1$, there is no problem in understanding the occurrence of synchronous motion for very small eccentricity, as can be also verified in Fig. 12.

It is important to note that instead to compute a critical C_{22} value, the condition for stationary solutions $\langle T_{\text{tide}} \rangle + \langle T_{22} \rangle = C\dot{\Omega} = 0$ also enables us to obtain a critical value of e for a given fixed C_{22}. The resonant motion would destabilize whenever the eccentricity becomes smaller than the critical value for each SOR. This approach is more convenient in those cases for which the observations allow an estimation of C_{22} [see Correia & Laskar (2004) for the study of the rotation of Mercury].

5 DISCUSSION AND CONCLUSIONS

The numerical exploration of the planet rotation which is subject to the conservative triaxial gravitational torque of the star shows different behaviours, including the oscillation around the equilibrium points of SORs (see Callegari & Rodríguez 2012 and references therein). When dissipative effects produced by tidal torques are included, the rotation of close-in bodies can be captured in a resonant motion (Goldreich 1966; Goldreich & Peale 1966; Celletti & Chierchia 2008). The capture in a specific resonance depends on the eccentricity e and on parameters related to tides and equatorial ellipticity (Q and C_{22}, respectively). Hence, since e is tidally damped during the inward migration, each specific capture should become unstable and the rotation can achieve another resonant state, which, at the same time, should result in a temporary trapping. When the orbit is circularized, the final evolution results in the synchronization between the orbital and rotational periods (i.e. the 1/1 SOR).

In this paper, we analysed the coupled spin–orbit evolution of Kepler-10 b, GJ 3634 b and 55 Cnc e short-period super-Earth planets. The numerical simulation of the exact equations of motion has shown that, depending on C_{22}, the rotation displays a number of resonance trappings for which $\Omega \simeq pn$, including the cases $p = 5/2$, 2, 3/2, 4/3 and 1. Moreover, the results indicate that GJ 3634 b can be an example of an exoplanet with a rotation state similar to Mercury's rotation ($p = 3/2$), provided the body figure can support a permanent equatorial asymmetry as small as $C_{22} = 10^{-5}$. 55 Cnc e

can currently evolve under 5/2 or 3/2 trappings if $C_{22} \sim 10^{-3}$ and under 2/1 if $C_{22} \sim 10^{-4}$ or even if C_{22} is as small as 2.45×10^{-5}. The rotation of 55 Cnc e may have a chaotic behaviour for $C_{22} \sim 10^{-3}$ (Callegari & Rodríguez 2012). However, we have shown that a scenario is possible in which the rotation evolves towards synchronism through successive trappings in SOR. Indeed, the eccentricity damping due to tides provides the destabilization mechanism required to escape from one given capture and subsequently evolves to lower order resonances (see Correia & Laskar 2004, 2009).

We have shown that different spin-states corresponding to various resonance captures can occur in extrasolar systems. Although the 1/1 spin–orbit coupling is the final state of evolution, it is not reached in every case as present configuration. For current non-circular orbits, trappings in the 3/2 SOR or other resonance configurations can be sustained over long times. The latter would depend on the orbital eccentricity, the planet's C_{22} value and its dissipation factor. Given that these parameters are not well-determined for terrestrial extrasolar planets, we note that the 1/1 coupling may not be the current rotation state of some planets. This would have consequences on the stellar insulation and therefore on the evolution of the atmosphere and surface of the planet.

When only the tidal torque is taken into account ($C_{22} = 0$), the rotation evolves to the STS. We have shown that under assumption of $C_{22} > 0$, the evolution along SOR leads to higher rates of orbital decay and circularization than the corresponding ones when the rotation evolves in the STS. Moreover, for a given C_{22} value, the variation rates of the elements depend on the specific trapping in which the rotation is trapped in, and increases with p (see Fig. 4).

We have also calculated the averaged rates of variations of semimajor axis and eccentricity including the gravitational and tidal torques. Moreover, through the analytical calculation of the critical value of C_{22} it is possible to predict the values of the eccentricity for which a given SOR would become unstable. The comparison with the direct numerical simulations has shown a good concordance for the analysed planets.

The importance of the C_{22} value on the rotational history of the planet is illustrated in the example of Kepler-10 b. It is worth noting that the planet rotation of Kepler-10 b can evolve under the influence of the 2/1 SOR for longer time-scales (i.e. small e) provided the planet figure can support a permanent equatorial deformation characterized by $C_{22} \sim 10^{-3}$. For smaller C_{22}, the 2/1 resonant state would become unstable for relatively large eccentricity (Figs 11 and 12).

We stress that the results of the numerical simulations provide different possible spin–orbit evolutions depending on the considered initial values of elements and rotation. The Q value and the specific tidal model would also play an important role in determining the rotation history of the planet, since the temporary trapping in SOR depends on the rate of eccentricity damping, which is Q-dependent. In fact, in a recent paper, Makarov (2012) has applied the model by Efroimsky (2012) and successfully explained the current resonant state of Mercury within the considered model.

Our results concerning the association of the critical C_{22} value with the capture probability are not new in the context of averaged equations of the spin–orbit problem (see e.g. Correia & Laskar 2004, 2009). However, in this work, we are able to compare the results of the averaged equations with those resulting from the numerical simulations of the exact equations of motion.

A model of planet interior including the effect of viscous friction at the core–mantle boundary would provide quantitatively different results (see Peale 2005; Correia & Laskar 2009, for the case of Mercury). According to previous works the chances of resonant capture increase if the latter effect is taken into account (Goldreich & Peale 1967). However, in order to highlight the contribution of C_{22} to the orbital evolution, in this paper we adopt a simple model neglecting a possible layered structure of the planet.

In the present study we have assumed constant C_{22} values. However, depending on the adjustment to hydrostatic equilibrium C_{22} may be itself time-dependent. The time-scale for adjustment to the completely relaxed state depends on material parameters, e.g. rigidity and viscosity, which are highly temperature dependent. Furthermore, it will depend on the spin–orbit coupling the planet is trapped in. For the application to terrestrial planets given here the constant, i.e. frozen, C_{22} configuration is justified because adjustment of solid rocky planets to equilibrium usually occurs on geological time-scales. Therefore, the states described here do not necessarily represent hydrostatic configurations.

In this work we have considered a model of one interacting planet, despite the fact that Kepler-10 b and 55 Cnc e belong to multipleplanet systems with exterior (more massive) companions. Previous works have shown that the mutual secular interaction with the companion may affect the eccentricity evolution of the tidally evolved planet, increasing the circularization time-scale (Mardling 2007; Rodríguez et al. 2011a; Rodríguez, Michtchenko & Miloni 2011b). Moreover, the planetary perturbations can produce large excursions of the innermost planet eccentricity, providing a mechanism for increasing or decreasing the capture probability of the SORs (Correia & Laskar 2004, 2009). However, a numerical simulation of 55 Cnc system including the exterior companion 55 Cnc b has shown little differences with the single planet case. Indeed, the evolution of the inner orbit eccentricity is almost not affected by the mutual interaction between the planets and thus the rotation evolution of 55 Cnc e can be safely analysed within the one-planet model. An investigation of the rotation of asymmetric close-in super-Earths including an exterior companion will be done in a future investigation.

ACKNOWLEDGMENTS

REFERENCES

Agnor C. B., Canup R. M., Levison H. F., 1999, Icarus, 142, 219
Batalha N. M. et al., 2011, ApJ, 729, 27
Beutler G., 2005, Methods of Celestial Mechanics, Vol. I. Springer, Berlin
Bonfils X. et al., 2011, A&A, 528, A111
Callegari N., Jr, Rodríguez A., 2012, preprint (arXiv:1205.5704)
Celletti A., Chierchia L., 2008, Celestial Mech. Dyn. Astron., 101, 159
Celletti A., Froeschlé C., Lega E., 2007, PASP, 55, 889
Correia A. C. M., 2006, Earth Planet. Sci. Lett., 252, 398
Correia A. C. M., Laskar J., 2004, Nat, 429, 848
Correia A. C. M., Laskar J., 2009, Icarus, 201, 1
Correia A. C. M., Laskar J., 2012, ApJ, 751, L43
Correia A. C. M., Levrard B., Laskar J., 2008, A&A, 488, L63
Danby J., 1962, Fundamentals of Celestial Mechanics. Macmillan, New York
Darwin G. H., 1880, Philos. Trans., 171, 713 [repr. Scientific Papers, Cambridge, Vol. II, 1908]
Dobbs-Dixon I., Lin D. N. C., Mardling R. A., 2004, AJ, 610, 464
Dobrovolskis A. R., 2007, Icarus, 192, 1
Efroimsky M., 2012, Celestial Mech. Dyn. Astron., 112, 283

Efroimsky M., Williams J. G., 2009, Celest. Mech. Dyn. Astron., 104, 257
Everhart E., 1985, in Carusi A., Valsecchi G. B., eds, Dynamics of Comets: Their Origin and Evolution. Reidel, Dordrecht, p. 185
Ferraz-Mello S., 2012, preprint (arXiv:1204.3957)
Ferraz-Mello S., Rodríguez A., Hussmann H., 2008, Celest. Mech. Dyn. Astron., 101, 171 [Erratum: 2009., Celest. Mech. Dyn. Astron., 104, 319]
Gillon M. et al., 2012, A&A, 539, A28
Goldreich P., 1966, AJ, 71, 1
Goldreich P., Peale S., 1966, AJ, 71, 425
Goldreich P., Peale S., 1967, AJ, 72, 662
Greenberg R., Weidenschilling S. J., 1984, Icarus, 58, 186
Heller R., Leconte J., Barnes R., 2011, A&A, 528, A27
Hut P., 1981, A&A, 99, 126
Iess L. et al., 2010, Sci, 327, 1367
Jackson B., Barnes R., Greenberg R., 2009, ApJ, 698, 1357
Kaula W. M., 1964, Rev. Geophys. Space Phys., 2, 661
Kokubo E., Ida S., 2007, ApJ, 671, 2082
Makarov V. V., 2012, ApJ, 752, 73
Mardling R. A., 2007, MNRAS, 382, 1768
Michtchenko T. A., Rodríguez A., 2011, MNRAS, 415, 2275
Mignard F., 1979, Moon Planets, 20, 301
Murray C. D., Dermott S. F., 1999, in Murray C. D., ed., Solar System Dynamics. Princeton Univ. Press, Princeton, NJ
Peale S. J., 2005, Icarus, 178, 4
Pettengill G. H., Dyce R. B., 1965, Nat, 206, 1240
Rodríguez A., Ferraz-Mello S., 2010, EAS Publ. Series, 42, 411
Rodríguez A., Ferraz-Mello S., Michtchenko T. A., Beaugé C., Miloni O., 2011a, MNRAS, 415, 2349
Rodríguez A., Michtchenko T. A., Miloni O., 2011b, Celestial Mechanics Dyn. Astron., 111, 161
Schubert G., Anderson J. D., Spohn T., McKinnon W. B., 2004, in Bagenal F., Dowling T. E., McKinnon W. B., eds, Jupiter. The Planet, Satellites and Magnetosphere, Vol. 1. Cambridge Univ. Press, Cambridge, p. 281
Smith D. E. et al., 2012, Sci, 336, 214
Tittemore W. C., Wisdom J., 1988, Icarus, 74, 172
Valencia D., 2011, in Sozzetti A., ed., Proc. IAU Symp. 276, The Astrophysics of Planetary Systems – Formation, Structure, and Dynamical Evolution. Cambridge Univ. Press, Cambridge, p. 181
Valencia D., Sasselov D. D., O'Connell R. J., 2007, ApJ, 665, 1413
Wieczorek M. A., Correia A. C. M., Le Feuvre M., Laskar J., Rambaux N., 2012, Nat. Geosci., 5, 18
Winn J. N. et al., 2011, ApJ, 737, L18
Wisdom J., 2008, Icarus, 193, 637

Table A1. Expansion of the function $H(p, e)$ given by equation (A1) for $\mathcal{O}(e^7)$ for the principal SORs.

p	$H(p, e)$
1	$1 - \frac{5}{2}e^2 + \frac{13}{16}e^4 - \frac{35}{288}e^6$
3/2	$\frac{7}{2}e - \frac{123}{16}e^3 + \frac{489}{128}e^5$
2	$\frac{17}{2}e^2 - \frac{115}{6}e^4 + \frac{601}{48}e^6$

APPENDIX A

We show here the explicit expressions for the functions $H(p, e)$ and $\mathcal{T}(p, e)$. The exact form of $H(p, e)$ is given by

$$H(p, e) = \frac{1}{\pi} \int_0^\pi \left(\frac{a}{r}\right)^3 \exp(i\,2f)\exp(i\,2p\,l)\,\mathrm{d}l. \tag{A1}$$

The expansion up to order six in e is displayed in Table A1 for $p = 1$, 3/2 and 2.

The exact expression for the function $\mathcal{T}(p, e)$ is given by (Hut 1981)

$$\mathcal{T}(p, e) = (1 - e^2)^{-6} \left[f_2(e) - (1 - e^2)^{3/2} f_5(e)\,p \right], \tag{A2}$$

where

$$f_2(e) = 1 + \frac{15}{2}e^2 + \frac{45}{8}e^4 + \frac{5}{16}e^6 \tag{A3}$$

and

$$f_5(e) = 1 + 3e^2 + \frac{3}{8}e^4. \tag{A4}$$

This paper has been typeset from a T$_{\!E}$X/LAT$_{\!E}$X file prepared by the author.